WP17ER-PR(18) 19274

M Idouakass et al.

Impurity density gradient influence on trapped particle modes

Preprint of Paper to be submitted for publication in
Physics of Plasmas

This work has been carried out within the framework of the EUROfusion Consortium and has received funding from the Euratom research and training programme 2014-2018 under grant agreement No 633053. The views and opinions expressed herein do not necessarily reflect those of the European Commission.

Impurity density gradient influence on trapped particle modes

M. Idouakass[1], E. Gravier[1], M. Lesur[1], J. Médina[1], T. Réveillé[1], T. Drouot[1], X. Garbet[2], Y. Sarazin[21]
[1] *Institut Jean Lamour, UMR 7198 CNRS, Université de Lorraine, 54000 Nancy, France*
[2] *CEA, IRFM, 13115, Saint-Paul-Lèz-Durance, France*

(Dated: 16 January 2018)

The effect of the presence of an impurity species on the trapped particle turbulence is studied using the gyrokinetic code TERESA, which allows the study of Trapped Electron Modes and Trapped Ion Modes. The impurity species is treated self-consistently and its influence on the nature of the turbulence, ion driven or electron driven, is investigated. It is found that the presence of heavy impurities with a flat density profile tends to stabilize the both electron and ion modes, whereas a peaked or hollow impurity density profile can change the turbulence from an electron driven turbulence to an ion driven turbulence. The effect of the turbulence regime on impurity transport is studied.

I. INTRODUCTION

In tokamak physics, impurities are defined as particles of the plasma that are not part of the elements that contribute to the reaction of fusion. Impurity transport is an issue that needs to be understood in order to obtain a sustainable burning plasma. These impurities can have different sources, they can come from the plasma boundaries, where particles are sputtered from the walls: In that case the impurity species will be tungsten in the context of ITER, or can be Carbon in other machines (such as JT60-SA). In addition, other species, such as argon or neon, can be introduced in the plasma edge in order to decrease the heat and particle fluxes on the walls, and these particles can then propagate into the plasma core. On the other hand, the impurities can come from the plasma core, in which case they are α-particles produced by the reactions of fusion.

These impurities can have negative effects on the plasma confinement in two major ways. First they may contribute to plasma dilution, reducing the fuel present for a given pressure. Second, these impurities are ionized multiple times, and through cycles of ionization-recombination and excitation-deexcitation, will radiate a significant part of the plasma energy from the core.

It is therefore very important to understand impurity transport so that accumulation in the plasma core can be avoided. The direction of such a transport depends on the direction of the impurity density gradient, and can vary when moving from ion dominant instabilities to electron dominant instabilities.

In this work, we look at the influence of the impurity profile on trapped particle driven modes, and study the transport of these impurities. This is done using the code TERESA, which is a semi-Lagrangian code based on a collisionless reduced bounce-averaged gyrokinetic model[1–6]. This code treats the passing particles adiabatically, and allows the study of Trapped Electron Modes (TEM) and Trapped Ion Modes (TIM). Its most interesting property is that it enables the full-f treatment of multiple populations of trapped particles at low numerical cost. However, the model on which the TERESA is based is collisionless, and as such it can only provide the turbulent contribution to transport.

In the high temperature and low collisionnality regime in which ITER is expected to be run, the collisionless turbulent transport contribution is expected to dominate over the neoclassical contribution for light impurities[7].

For heavy impurities, while the contribution of neoclassical (collisional) transport, and the interplay between turbulent and neoclassical transport[8], need to be taken into account to have a complete understanding of impurity transport, obtaining a clear picture of the purely turbulent impurity transport is a necessary step towards that complete understanding.

TERESA allows the processing of trapped ions, electrons, and impurities. This enables us to observe the action of the impurities as an active species, i.e. taken into account in the quasineutrality constraint, thus seeing how they influence the dynamics of the plasma, particularly on the instability growth rates and on the nonlinear phase. We will show that by changing the radial gradient of impurities in an otherwise identical plasma, it is possible to move from a situation where TEMs dominate the dynamics to a situation where TIMs dominate. In addition, we show that depending on the dominant regime of turbulence, the importance of the zonal flow and thus of transport changes.

In section II, the model used in this paper is briefly described, then it is used to perform the linear analysis in section III where it is shown how impurities modify the linear growth rate of the instability. In section IV, the simulation parameters and numerical results on zonal flow generation and transport are discussed. Finally, a brief summary of the results along with a conclusion are given.

II. MODEL - TERESA CODE

The code TERESA is based on an electrostatic reduced bounce averaged gyrokinetic model[1,6,9,10]. The dynamics that will be considered here evolve on timescales of the order of the trapped particles precession frequency. Therefore it is possible to gyro-average and bounce-average the

Vlasov equation, thus filtering out the fast frequencies ω_C (cyclotron frequency) and ω_b (bounce frequency) and the small space scales ρ_c (gyro-radius) and δ_b (banana width). The trapped particles are treated kinetically, while the passing particles are treated adiabatically.

This allows one to reduce the dimensionality from 6D to 4D. It is furthermore possible to adopt an action-angle formalism, simplifying the treatment of the Vlasov equations. Finally only two variables appear in the differential operators: the angle $\alpha = \varphi - q\theta$ and the magnetic flux ψ where φ is the toroidal angle, θ is the poloidal angle, and q is the safety factor. The variable ψ is a function of the minor radius, and will be used as a radial coordinate for the numerical simulations. The other two dimensions are two invariants: the particle kinetic energy E and the trapping parameter $\kappa = \sqrt{\frac{1-\lambda}{2\varepsilon\lambda}}$ where $\lambda = \mu B_{\min}/E$, μ is the magnetic moment, $B_{\min}$ is the minimum magnetic field amplitude, and $\varepsilon = a/R_0$ is the inverse aspect ratio (a being the minor radius and R_0 the major radius at the magnetic axis).

Using these reductions, the Vlasov equation reads:

$$\frac{\partial f_s}{\partial t} - [J_{0,s}\phi, f_s]_{\alpha,\psi} + \omega_d \frac{\partial f_s}{\partial \alpha} = 0 \tag{1}$$

Here, f_s is the gyro-averaged particle distribution function, with the subscript $s = i, e, z$ indicating the species considered (main ion, electron, or impurity), and ϕ is the plasma potential. The Poisson brackets are defined as $[g,h] = \partial_\alpha g \partial_\psi h - \partial_\alpha h \partial_\psi g$. $\omega_{d,s} = \frac{\Omega_d E}{Z_s}$ is the precession frequency where Z_s is the charge number and Ω_d is a normalized pulsation that depends on the magnetic shear and on the trapping parameter κ. In this paper, we will assume that the magnetic shear is constant over radius and that there is a single value $\kappa = 0$, corresponding to deeply trapped particles. This further reduces the dimensionality from 4D to 3D. The gyro-bounce-averaging operator is approximated as

$$J_{0,s} = \left(1 - \frac{E}{T_{eq,s}} \frac{\delta_{b0,s}^2}{4} \partial_\psi^2\right)^{-1} \left(1 - \frac{E}{T_{eq,s}} \frac{q^2 \rho_{c0,s}^2}{4a^2} \partial_\alpha^2\right)^{-1} \tag{2}$$

where $\rho_{c0,s}$ and $\delta_{b0,s}$ are the Larmor radius and the banana width at an arbitrary typical temperature T_0, $\delta_{b0,s} = q\rho_{c0,s}/\sqrt{\varepsilon}$ and $T_{eq,s}$ is the equilibrium temperature at $\psi = 0$.

The quasi-neutrality equation reads

$$\frac{2}{\sqrt{\pi}} \frac{T_{eq,i}}{T_0} \sum_s \left(Z_s \mathscr{C}_s \int_0^\infty J_{0,s} f_s E^{1/2} dE \right) = C_{ad} \left(\phi - \varepsilon_\phi < \phi >_\alpha\right) - C_{pol} \sum_s \mathscr{C}_s \tau_s Z_s^2 \Delta_s \phi \tag{3}$$

where $\mathscr{C}_s = n_s/n_{eq}$ is the concentration (n_s is the population density, $n_{eq} = n_{0,e}$ is the equilibrium density, and we have $\sum_s Z_s n_s = 0$), $C_{pol} = e\omega_0 L_\psi / T_0$ where ω_0 is a typical precession frequency and L_ψ is the radial simulation box length (in units of ψ), $C_{ad} = C_{pol} \frac{1-f_T}{f_T} \sum_s (Z_s \mathscr{C}_s \tau_s)$ where f_T is the fraction of trapped particles and $\tau_s = T_{eq,i}/T_s$. The operator Δ_s is defined as $\Delta_s = \left(\frac{q\rho_{c0,s}}{a}\right)^2 \partial_\alpha^2 + \delta_{b,0}^2 \partial_\psi^2$ and $\epsilon_\phi = (\sum_s \tau_s \mathscr{C}_s Z_s^2 \varepsilon_{\phi,s})/(\sum_s \tau_s \mathscr{C}_s Z_s^2)$. ϵ_ϕ is a control parameter which governs the response of the adiabatic passing particles. Regarding the electron response, $\epsilon_{\phi,e} = 1$ prevents the passing electrons from responding to the zonal potential which is constant on a flux surface (toroidal mode $n = 0$). This situation prevails when the electron gyroradius is small compared with the characteristic length of the zonal flows[11]. Unlike passing electrons, passing ions must respond to zonal flows ($0 \leq \epsilon_{\phi,i} \leq 1$), therefore ϵ_ϕ should be in the range $[0, 1]$. The model does not allow the adiabatic response to be properly computed so we introduce ϵ_ϕ as a free parameter and assume the form chosen in Eq. (3). A detailed study of this parameter was performed in ref.[12]. Hereafter, only the extreme case $\epsilon_\phi = 1$ is considered.

III. LINEAR THEORY

A. Dispersion relation

Linearizing eqs. (1) and (3) yields a linear dispersion relation which can be solved to find the growth rate and real frequency of the TEM and TIM for different plasma parameters. The dispersion relation reads:

$$D = 0 = C_n - \sum_s \mathscr{C}_s \tau_s \int_0^\infty J_{n,s}^2 \frac{\kappa_{n,s} + \kappa_{T,s}(\xi_s - \frac{3}{2})}{\Omega_d(\xi_s - W_s)} \mathrm{e}^{-\xi_s} \xi_s^{\frac{1}{2}} d\xi \tag{4}$$

where the equilibrium distribution function has been approximated by

$$F_{eq,s} = \frac{n_{0,s}}{T_{eq,s}^{\frac{3}{2}}} \mathrm{e}^{-\xi_s} \left[1 + \psi \left(\kappa_{n,s} + \kappa_{T,s}(\xi_s - \frac{3}{2})\right)\right] \tag{5}$$

and the coefficient C_n is defined as $C_n = \frac{\sqrt{\pi}}{2} \left[C_{ad} + C_{pol} n^2 \sum_s \mathscr{C}_s \tau_s Z_s^2 \rho_{C,s}^2 + C_{pol} k^2 \sum_s \mathscr{C}_s \tau_s Z_s^2 \delta_{b,s}^2\right]$. Here, $\xi = \frac{E}{T_{eq,s}}$, $W_s = \frac{Z_s \omega}{n \Omega_d T_s}$, n being the mode number in the α-direction, $k = \pi$ the most unstable radial mode and ω the mode frequency. The inverse radial gradient lengths are given by $\kappa_{n,T} = \partial_\psi \log(n_{eq}, T_{eq})$.

B. Presence of an impurity species

Using this dispersion relation, we will investigate the effect of introducing an impurity species. Here and in the remainder of the paper, we consider a plasma composed of deuterium as the single main ion species and tungsten W^{40+} as a single impurity species.

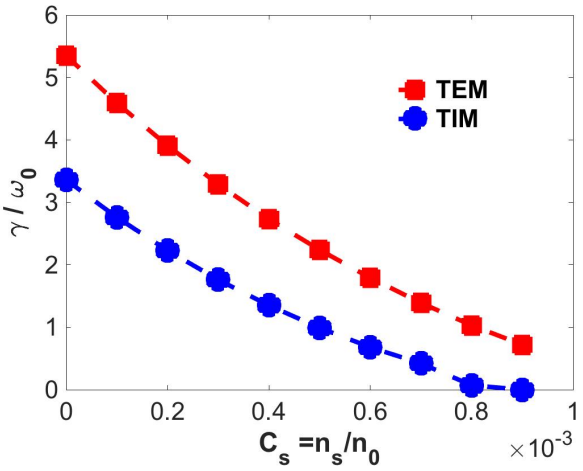

FIG. 1. Growth rate of the fastest growing mode of TIMs and TEMs as a function of the tungsten impurity density. The blue dots correspond to TIM growth rates, the red dots correspond to TEM growth rates.

TABLE I. Typical plasma parameters used.

$n_{e,0}$	$\rho_{c,e}$	$\rho_{c,i}$	$\rho_{c,z}$	$\delta_{b,e}$	$\delta_{b,i}$	$\delta_{b,z}$	$\kappa_{T,s}$	$\kappa_{n,s}$	τ_e	τ_z
1	0.01	0.03	0.0072	0.01	0.1	0.024	0.25	0	1	1

1. Impurities with no radial density gradient

Let us first look at a situation where there is no radial density gradient. For the parameters shown in Table I, Fig. 1 shows the growth rate of TIMs and TEMs as a function of the concentration.Consistently with ref.[13–16], we observe that the impurities, for flat density profiles, have a stabilizing effect on trapped particle modes due to increased dilution, and that this stabilizing effect increases with the impurity concentration. Although it is not shown here, we observed that the TIMs and TEMs are stabilized more easily by impurity species with higher charge number.

2. Influence of the radial density gradient

We will now look at the influence of a radial density gradient of impurities. For this study, the density profile of electrons is fixed, the impurity profile is varied, and the main ion profile is adapted to ensure quasi-neutrality. Let us first define the relative impurity gradient length as $G_Z = \kappa_{n,z}/\kappa_{n,e}$. The parameters of the simulations shown in this section are displayed in Table II. The parameters not shown are the same as in Table I.

We show two cases in Fig. 2, corresponding to a population of tungsten impurities with the same concentration, but opposite gradients $G_Z = \pm 20$. Note that this value is large mainly because $\kappa_{n,e}$ is small. In that situation, the linear analysis shows that for an impurity profile

TABLE II. Parameters for cases with an impurity density gradient.

$\kappa_{n,i}$	$\kappa_{n,e}$	$\mathscr{C}_i$	$\mathscr{C}_z$	$\mathscr{C}_e$
0.05	0.05	0.968	0.0008	1

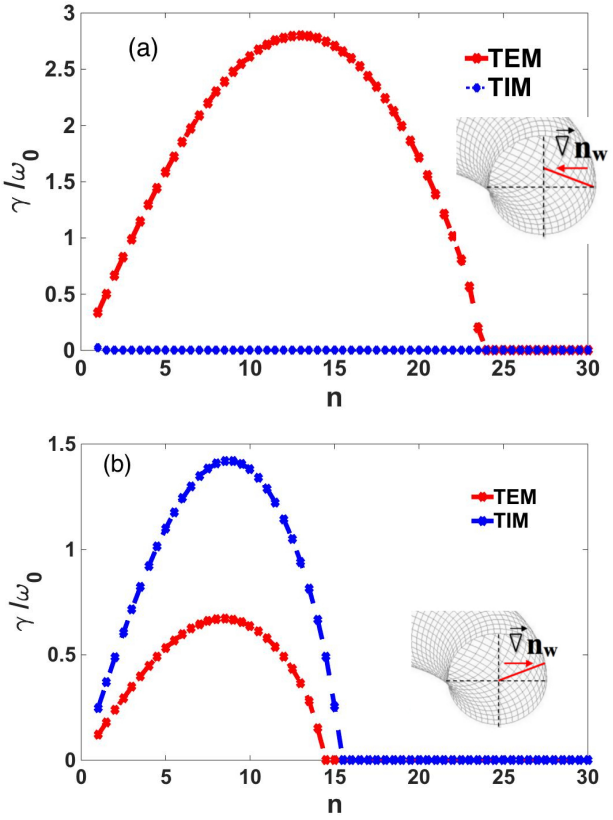

FIG. 2. Growth rate of TEMs and TIMs as a function of mode number. Case (a): $G_Z = 20$, case (b): $G_Z = -20$. The blue dashed curve corresponds to the growth rate of the TIM modes, the red solid curve corresponds to the growth rate of the TEM modes. For clarity, negative growth rates have been set to zero. The poloidal cross section sketches display the shape of the impurity profile for negative and positive G_Z.

peaked ($G_Z > 0$) the TEMs are the most linearly unstable (see Fig. 2(a)). On the other hand, when the impurity profile is hollow ($G_Z < 0$), the TIMs are the most linearly unstable (see Fig. 2(b)). It is quite interesting to see that the gradient of heavy impurities, when it is in the same direction as the main ion species gradient, will decrease the TIM growth rate and increase the TEM growth rate, whereas it will increase the TIM growth rate and decrease the TEM growth rate when these gradients are in opposing directions. This result is consistent with results from non bounce-averaged gyrokinetic simulations discussed in refs.[13,16], where it was shown that the TEM growth rate increases with the impurity density gradient in the case of a relatively flat electron density profile. This trend is also observed in Fig. 3, which displays the

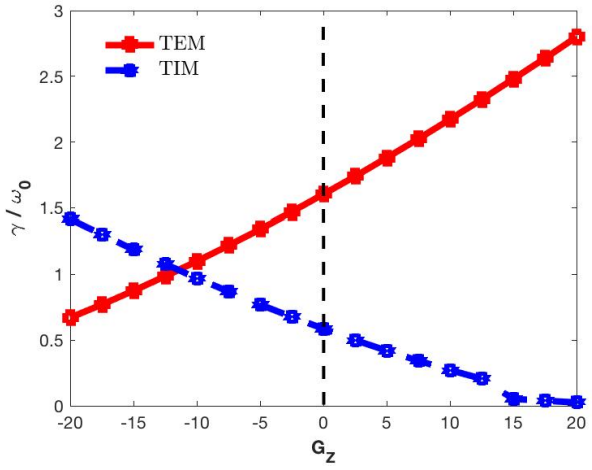

FIG. 3. Linear growth rate of the fastest growing mode as a function of the impurity gradient length G_Z. The blue dashed curve corresponds to TIM growth rates, the red solid curve corresponds to TEM growth rates.

linear growth rate of the fastest growing TIM and TEM for different impurity density gradients. In addition, we can see in Fig. 3 a transition between TIM dominated dynamics and TEM dominated dynamics occuring around $G_Z = -12$ for the parameters considered here.

IV. NONLINEAR SIMULATIONS

The numerical simulations are done using a thermal and density bath as boundary conditions, i.e. the temperature and density are fixed at both radial boundaries $\psi = 0$ (outer boundary) and $\psi = 1$ (inner boundary). Dirichlet boundary condition are imposed on the potential. The grid mesh is $N_\alpha = 257$, $N_\psi = 513$, and $N_E = 192$ for the energy parameter. An initial perturbation is imposed on the electrostatic potential, with all modes excited with a small amplitude and a random phase.

First, let us note that there is a good agreement between the linear analysis prediction for the growth rates and the ones obtained from direct, initial value, numerical simulations. In addition, the direction of propagation of the instability (ion precession direction for TIMs and electron precession direction for TEMs) is recovered, depending on the inward ($G_Z = +20$) or outward ($G_Z = -20$) impurity density gradient. There is a small difference in the numerical and analytical linear growth rates, leading to a transition from TIM dynamics to TEM dynamics for $G_Z \simeq -14$ numerically. This difference is due to the assumptions made in the linear theory.

A. Influence of the dominant mode on the zonal flow

An interesting quantity to consider when investigating the importance of the zonal flow is its energy compared to that of the other modes. This ratio can be calculated as[5]:

$$\frac{W_{ZF}}{W_{n\neq 0}} = \frac{\int_0^1 \left\langle \frac{\partial \phi}{\partial \psi} \right\rangle_\alpha^2 d\psi}{\int_0^1 \left\langle \left(\frac{\partial \phi}{\partial \psi} - \left\langle \frac{\partial \phi}{\partial \psi} \right\rangle_\alpha \right)^2 \right\rangle_\alpha d\psi} \tag{6}$$

where W_{ZF} is the zonal flow energy and $W_{n\neq 0}$ is the energy contained in all other modes.

In Fig. 4, the time evolution of the amplitude of different modes is given, and the zonal flow amplitude is highlighted. The two cases shown here are the ones discussed previously. In the saturated phase, we observe that the ratio $W_{ZF}/W_{n\neq 0}$ is much larger when TIMs dominate the dynamics than when the TEMs dominate the dynamics. In the case $G_Z = -20$ (TIM), the ratio is $W_{ZF}/W_{n\neq 0} \simeq 3500$, while in the case $G_Z = +20$ (TEM), the ratio is $W_{ZF}/W_{n\neq 0} \simeq 80$.

It appears, consistently with ref.[11], that the important factor to look at for the order of magnitude of this ratio is not the sign of the gradient of impurities, but whether the dominant mode is an electron or an ion driven mode, which itself depends on the impurity profile. For example, in the case of a hollow impurity profile, with $G_Z = -5$, the dominant mode is a TEM and the ratio is of the order of $W_{ZF}/W_{n\neq 0} \simeq 100$.

It should be noted that these ratios are high in all cases due to the parameters chosen, so the ratios are relevant considered with respect to one another.

B. Impurity transport

In this section, we will investigate the transport of particles when impurities are present. The particle flux is defined as[6]

$$\Gamma_s = -\frac{2}{\sqrt{\pi}} \int d\alpha \int \frac{\partial J_{0,s}\phi}{\partial \alpha} f_s E^{\frac{1}{2}} dE \tag{7}$$

The particle flux can be modelled as the sum of a diffusive flux and a convective flux

$$\Gamma_s = -D_s \nabla n_s + V_s n_s \tag{8}$$

where D_s is a diffusion coefficient and V_s is a pinch velocity.

We first note that when there is a inward gradient of impurities ($G_Z > 0$), the TEMs dominates the dynamics and the transport is dominated by the electrons. In that case, the impurities particle and heat fluxes are outward.

On the other hand, when there is an outward gradient of impurities, either the TIMs or the TEMs can dominate the dynamics, but in both cases, the impurity particle flux is inward.

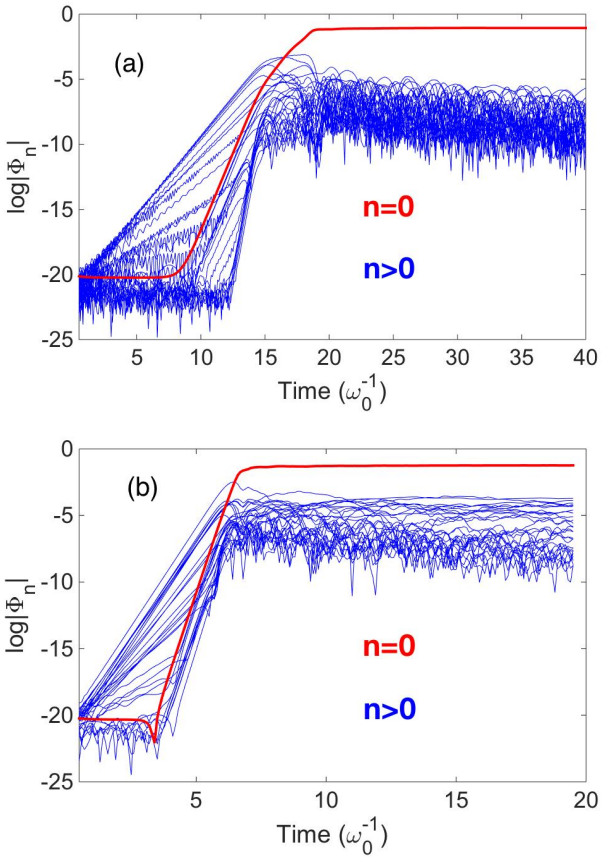

FIG. 4. Temporal evolution of the potential amplitude, for $n = 0$ to $n = 30$. The mode $n = 0$ is highlighted in red. Case (a): $G_Z = -20$ where TIM are dominant, case (b): $G_Z = +20$ where TEMs are dominant.

Fig. 5 shows the impurity particle flux Γ_z, averaged over the spatial variables, and averaged over time, as a function of G_Z. We see that there are different transport regimes depending on the radial impurity density gradient.

Let us first look at the range $-20 < G_Z < -15$. This is a range of parameters where the TIMs are dominating the dynamics, and we can see that there is a very weak dependence of the transport on the impurity density gradient. We note here that the particle flux does not scale linearly with the gradient, which would seem to indicate that in that regime, there is a significant inward pinch.

In the next range, $-15 < G_Z < -12$, there is a competition between the TIMs and the TEMs, and we can observe a strong decrease of the transport with a small increase of the gradient. This is likely due to a transition from the ion driven to the electron driven turbulent regime.

This leads to a range $-12 < G_Z < +6$ where the particle flux scales close to linearly, but there is a change of transport coefficient depending on the sign of the G_Z, with a transport coefficient in the peaked profile larger than in the hollow profile. However, the transition from

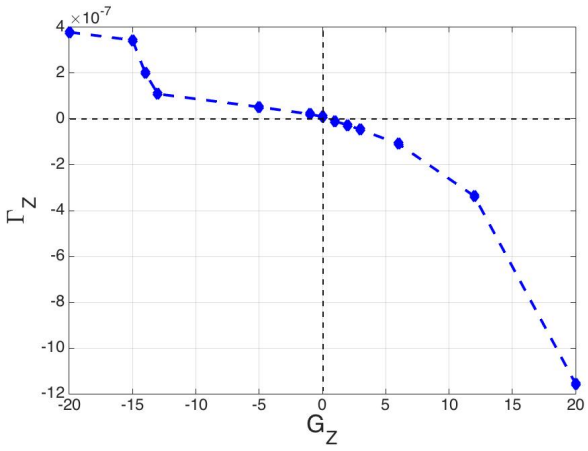

FIG. 5. Averaged impurity flux Γ_z as a function of G_Z. The dots correspond to simulation points.

inward to outward transport occurs very close to $G_Z = 0$, which indicates that there is no pinch in that turbulent regime. Ideed, in a zero-flux situation, the pinch velocity can be obtained as $V_s = (D_s \nabla n)/n$, which is zero for a flat density profile.

Then in the range $+6 < G_Z < +20$, the transport increases with a rate faster than linear with respect to G_Z. This is likely due to the appearence of an outward pinch increasing with G_Z and needs further investigation.

V. CONCLUSION

In this paper, we have studied the impact of the presence of a population of impurities in a tokamak plasma using the gyrokinetic code TERESA. We have shown that their presence can have a strong influence on the dynamics of the turbulence in the plasma. In particular, it was shown that the direction of the radial gradient of impurities could change the nature of turbulence, going from an electron dominated turbulence when the impurity density profile is peaked on the magnetic axis to a trapped ion mode turbulence when the impurity density profile is hollow. It was also shown that the nature of the turbulence could have a strong influence on the relative importance of the zonal flow energy compared to the energy contained in the turbulence, where for ion mode dominated turbulence, the ratio of zonal flow energy to turbulent energy is much greater than in electron mode dominated turbulence. Finally, we saw that in the case considered here, there was no impurity pinch for a zero-flux situation. In light of these results, it is clear that it is very important when looking at the dynamics of impurities to treat them self-consistently, as their effect on the turbulence can strongly affect their transport.

ACKNOWLEDGMENTS

This work was granted access to the HPC ressources of IDRIS under the allocation 2017-27862 made by GENCI (Grand Equipement National de Calcul Intensif). This work has been carried out within the framework of the EUROfusion Consortium and has received funding from the Euratom research and training programme 2014-2018 under grant agreement No 633053 for the project WP17-ENR-CEA-02. The views and opinions expressed herein do not necessarily reflect those of the European Commission.

[1] T. Drouot, E. Gravier, T. Reveille, A. Ghizzo, P. Bertrand, X. Garbet, Y. Sarazin, and T. Cartier-Michaud. A gyro-kinetic model for trapped electron and ion modes. *The European Physical Journal D*, 68(10):280, 2014.

[2] T. Drouot, E. Gravier, T. Reveille, and M. Collard. Self-generated zonal flows in the plasma turbulence driven by trapped-ion and trapped-electron instabilities. *Physics of Plasmas*, 22(10):102309, 2015.

[3] T. Drouot, E. Gravier, T. Reveille, M. Sarrat, M. Collard, P. Bertrand, T. Cartier-Michaud, P. Ghendrih, Y. Sarazin, and X. Garbet. Global gyrokinetic simulations of trapped-electron mode and trapped-ion mode microturbulence. *Physics of Plasmas*, 22(8):082302, 2015.

[4] E. Gravier, M. Lesur, T. Reveille, and T. Drouot. Stimulated zonal flow generation in the case of tem and tim microturbulence. *Physics of Plasmas*, 23(9):092507, 2016.

[5] E. Gravier, M. Lesur, T. Reveille, T. Drouot, and J. Mdina. Transport hysteresis and zonal flow stimulation in magnetized plasmas. *Nuclear Fusion*, 57(12):124001, 2017.

[6] Y. Sarazin, V. Grangirard, E. Fleurence, X. Garbet, P. Ghendrih, P. Bertrand, and G. Depret. Kinetic features of interchange turbulence. *Plasma Physics and Controlled Fusion*, 47:1817, 2005.

[7] C. Angioni, R. Bilato, F.J. Casson, E. Fable, P. Mantica, T. Odstrcil, M. Valisa, ASDEX Upgrade Team, and JET Contributors. Gyrokinetic study of turbulent convection of heavy impurities in tokamak plasmas at comparable ion and electron heat fluxes. *Nuclear Fusion*, 57(2):022009, 2017.

[8] X. Garbet, J.-H. Ahn, S. Breton, P. Donnel, D. Esteve, R. Guirlet, H. Lütjens, T. Nicolas, Y. Sarazin, C. Bourdelle, O. Février, G. Dif-Pradalier, P. Ghendrih, V. Grandgirard, G. Latu, J.F. Luciani, P. Maget, A. Marx, and A. Smolyakov. Synergetic effects of collisions, turbulence and sawtooth crashes on impurity transport. 2016. working paper or preprint.

[9] G. Depret, X. Garbet, P. Bertrand, and A. Ghizzo. Trapped-ion driven turbulence in tokamak plasmas. *Plasma Physics and Controlled Fusion*, 42(9):949, 2000.

[10] T. Cartier-Michaud, P. Ghendrih, Y.razin, G. Dif-Pradalier, T. Drouot, D. Estve, X. Garbet, V. Grandgirard, G. Latu, C. Norscini, and C. Passeron. Staircase temperature profiles and plasma transport self-organisation in a minimum kinetic model of turbulence based on the trapped ion mode instability. *Journal of Physics: Conference Series*, 561(1):012003, 2014.

[11] X. Garbet, Y. Idomura, L. Villard, and T.H. Watanabe. Gyrokinetic simulations of turbulent transport. *Nuclear Fusion*, 50(4):043002, 2010.

[12] T. Cartier-Michaud, P. Ghendrih, V. Grangirard, and G. Latu. Optimizing the parallel scheme of the poisson solver for the reduced kinetic code teresa. *ESAIM:Proc.*, 43:274, 2014.

[13] H. Du, Z.-X. Wang, J. Q. Dong, and S. F. Liu. Coupling of ion temperature gradient and trapped electron modes in the presence of impurities in tokamak plasmas. *Physics of Plasmas*, 21(5):052101, 2014.

[14] R.R. Dominguez and M.N. Rosenbluth. Local kinetic stability analysis of the ion temperature gradient mode. *Nuclear Fusion*, 29(5):844, 1989.

[15] R. Paccagnella, F. Romanelli, and S. Briguglio. Toroidal i mode stability in a multispecies plasma. *Nuclear Fusion*, 30(3):545, 1990.

[16] H. Du, Z.-X. Wang, and J. Q. Dong. Impurity effects on trapped electron mode in tokamak plasmas. *Physics of Plasmas*, 23(7):072106, 2016.